# A Hybrid Elastic Net-ANN Approach for Modeling the Ethanol-Methanol Mixture Concentration

Suryasatriya Trihandaru, Hanna Arini Parhusip, Devina Intan Sari

Abstract— Volatile mixture evaporation is crucial to be understood for industrial purposes, especially in fuel, food, and chemical processing. Evaporation of ethanol-methanol is examined in this research with a capacitive soil moisture sensor (CSMS) and a built-in heater. The experiment enables real time monitoring of evaporation by measuring voltage, and the concentration of the mixture is indirectly determined. Classical and deep learning regression models were used for the prediction of ethanol-methanol concentrations. Elastic Net regression reduced dimensionality with minimal performance loss, while ANNs captured nonlinear trends effectively. The highest performance was achieved with a hybrid Elastic Net-ANN model using 14 features that had a coefficient of determination (R2) of 0.99631 and minimal error rates. A simplified ANN statistical model with only seven statistics features provided robust results with R<sup>2</sup> of 0.9421, confirming its efficiency to describe critical evaporation features under lower complexity. Additionally, evaporation dynamics were modeled using both linear (d2-law) and nonlinear exponential models. Both models vielded effective evaporation rates around 0.001, demonstrate the applicability of capacitive sensing and machine learning for real-time, non-destructive, and accurate volatile mix analysis. They can be used to optimize industry processes, performing correct concentration estimations without relying on traditional gas chromatographic techniques.

Index Terms— Ethanol, methanol, Elastic Net-ANN, regression, evaporation

### I. INTRODUCTION

Understanding the dynamics of volatile evaporation is crucial in many industrial and research processes. Fitting experimental data to models that depict the evaporation time curve is necessary to gain this understanding. The parameters obtained from these models offer insights into various factors influencing the evaporation process, such as temperature, fluid concentration, and environmental conditions. Accurately determining these parameters allows for predicting the effects of different treatments and optimizing the process. Mixing different fluids is essential in many industrial and

Manuscript submitted April 18, 2025; revised September 21, 2025. Suryasatriya Trihandaru is an associate professor of Satya Wacana

Christian University, Indonesia (e-mail: suryasatriya@uksw.edu).

Hanna Arini Parhusip is a professor of Satya Wacana Christian
University, Indonesia (corresponding author e-mail: hanna.parhusip@ukse.edu).

Devina Intan Sari is a Master's graduate in Data Science from Satya Wacana Christian University, Indonesia (e-mail:devinais9906@gmail.com).

commercial applications to achieve the required properties and performance.

This is particularly important for industries such as chemicals, food, and fuel. For instance, this paper examines the mixture of ethanol and methanol. Both ethanol and methanol are alcohols with various industrial and commercial applications. These mixtures are particularly significant in the food industry, pharmaceuticals, and chemical manufacturing.

Ethanol and methanol are very useful solvents in food industry for extracting flavors and aromas. Both alcohols also have antimicrobial properties, which are beneficial for preserving food and sanitizing products. However, methanol is toxic to humans, necessitating careful control of its presence in food products to avoid health hazards. Both ethanol and methanol are volatile, and their volatility can be utilized to predict the concentration in their mixtures. This study demonstrates how to measure the concentration indirectly by assessing volatility through electronic devices.

Ethanol and methanol have distinct physical properties that significantly influence their behavior in mixtures. These properties include boiling temperature, dielectric constant, and volatility rate. Ethanol boiling point is 78.37°C, while methanol boiling point is around 64.7°C. Ethanol dielectric constant is 24.3 and methanol dielectric constant is 32.6. Additionally, the volatility rate between the two alcohols impacts the evaporation speed of the substances.

This research employs a novel technique to measure the evaporation dynamics of ethanol and methanol mixtures using a capacitive sensor. Specifically, it utilizes the voltage measurement of a capacitor filled with droplets of ethanol-methanol mixture. Time series formed from voltage readings presents the evaporation process. This study hypothesizes that the evaporation rate depends on the concentration of the components in the mixture.

Monitoring the voltage change over time makes it possible to determine the evaporation rate, and consequently, the concentration of ethanol and methanol in the mixture. This method offers a non-invasive and efficient means of studying volatile evaporation and could be applied to similar systems. The research result has potential applications in optimizing industrial processes and improving the accuracy of mixture concentration measurements in various fields.

Further exploration made to predict mixture concentration from time series data, firstly using Partial Least Squares Regression (PLSR) to extract and correlate the most relevant information from the voltage signals. PLSR is particularly effective in handling multicollinearity, non-normal

distribution, and uncertainty of factor results, making it suitable for analyzing complex sensor responses related to mixture compositions [1]. By reducing the dimensionality of the data while preserving variance relevant to the target concentrations, PLSR serves as a foundational model for comparative analysis.

Regression methods are also employed to achieve accurate predictions. Specifically Elastic Net with varying  $L_1$  and  $L_2$  regularization values and Artificial Neural Networks (ANNs) [2]. Elastic Net combines the properties of both Lasso and Ridge regression, allowing variable selection and regularization to enhance prediction accuracy. Adjusting the  $L_1$  and  $L_2$  allows us to fine-tune the model to capture the most relevant features. Additionally, ANNs offer powerful tool for capturing complex, non-linear relationship within the data.

In order to better comprehend the underlying evaporation mechanism, this study also looks at the modeling of capacitance decay related to mass loss. Most previous researches on the evaporation dynamics of ethanol, methanol, and their mixtures, have relied on linear models such as the classical d²-law, which assumes constant evaporation rate over the droplet's lifetime. However, recent findings, including experiments on water-ethanol systems at ambient conditions suggest more complex evaporation profiles, particularly in binary systems [3].

Building upon this, the present study purposes a nonlinear model to describe capacitance decay during evaporation, which is more representative of the actual mass loss process in volatile binary mixtures. Unlike conventional models that focus solely on flux estimations, this approach integrates dielectric measurements as a proxy for material quantity and enables more flexible curve fitting. Thus, this model captures better evaporation dynamic under moderate heating condition (e.g., 43°) and accounts for composition dependent behaviors not addressed in existing linear frameworks.

This study will also discuss the fitting method models to experimental data by optimizing the mean squared error (MSE), a measure of accuracy that frequently used for the method [4][5]. Finally, we will evaluate the goodness of fit using metrics such as the coefficient of determination ( $R^2$ ). These evaluation methods help in comparing the models and selecting the one that best describes the evaporation process.

By training the network on the optimal parameters, we can predict the mixture ratio with high accuracy. These approaches provide the novelty of this research, i.e., the behavior of ethanol-methanol mixtures, ultimately contributing to better control and optimization in various industrial applications.

# II. MODELLING PROCESS

#### A. Materials

The data used in this study consist of evaporation time series measurements of ethanol-methanol mixtures for regression analysis. Measurements were conducted using an Arduino microcontroller connected to a capacitive soil moisture sensor (CSMS). The CSMS was used to determine the evaporation rate over time based on changes in electrical conductivity during evaporation. It also measured the differences in electrical conductivity of the pure substances,

namely ethanol 99% and methanol 99%, for classification purposes. The ethanol-methanol mixtures were labeled based on their composition as 1.0, 0.8, 0.6, 0.4, 0.2, and 0.0. Here, 1.0 represents pure ethanol (99%), and 0.0 represents pure methanol (99%). Labels 0.8, 0.6, and 0.4 represent mixtures containing 80%, 60%, and 40% ethanol and 20%, 40%, and 60% methanol, respectively.

A BME280 temperature sensor was also employed to monitor the environmental conditions affecting the evaporation rate, particularly temperature, which was included in the regression analysis. Additionally, the actual ethanol and methanol concentrations were validated using Gas Chromatography (GC). The evaporation rates for each sample, measured as time series data, were analyzed using machine learning and neural networks (NN) for regression based on the sample's composition. [6] developed a two-phase numerical model to simulate the transient vaporization of spherical, two-component liquid fuel droplets, considering variations in thermo-physical properties, multicomponent diffusion, and surface tension. However, this mathematical model is much more expensive than some empirical models proposed in this paper.

Measurement of the content of ethanol and methanol is usually done using gas chromatography, as given by [7] This study introduces a rapid gas chromatography method to simultaneously measure ethanol and methanol in wines. Using a small sample (10  $\mu L)$  in a headspace vial at  $105^{\circ}C$ , it achieves precise measurement within three minutes. The results demonstrate high accuracy with reproducibility values of 1.02% for ethanol and 2.11% for methanol, and recoveries between 96.1% and 104%. This method is efficient for quality control in wine production.

Instead of using the gas chromatography technique, Effective Chemical Information (ECI) models using nearinfrared (NIR) spectra for identifying and analyzing methanol and ethanol in gasoline were developed [8]. Using PLS-DA and PLS algorithms, the ECI models achieved 100% accuracy in identifying methanol and ethanol gasoline. The ECI-PLS models also showed the lowest RMSEP for quantitative analysis. The ECI model demonstrated superior recognition and accuracy compared to other spectral models, making it a promising tool for rapid, accurate fuel analysis. An example of a dynamic model related to volatility, who analyzed the volatility and droplet evaporation dynamics of hydrous and anhydrous ethanol-gasoline blends using advanced distillation curves. The authors used only 3 different blends unsuitable for regression analysis [9].

Artificial Neural Network (ANN) models were developed to optimize ethanol/gasoline dual fuel spark ignition (DFSI) engines, which require complex calibration [10]. The study proposed ANN topologies to model performance, combustion characteristics, and emissions, achieving high accuracy with regression values between 0.9387 and 0.9962 and mean square relative errors between 0.000184 and 0.03935. These ANN models demonstrated strong robustness and reliability, beneficial for engine calibration and optimization.

# B. Ethanol-Methanol Measurement with Capacitor

The ethanol concentration in an ethanol-methanol mixture was indirectly measured using a capacitive soil moisture sensor (CSMS v2.0). This sensor utilizes a TL555I oscillator operating at a frequency of f = 1.5 MHz. The CSMS output

voltage is derived from frequency conversion based on Equation (1), i.e.,

$$V_{out} = \frac{V_{peak}}{\sqrt{1 + (2\pi fRC)^2}} \tag{1}$$

The capacitance C can be modified by introducing a dielectric material into the capacitor. Assuming the capacitor is parallel-plate with a cross-sectional area A and a separation distance d, the capacitance formula is expressed as:

$$C = \frac{\kappa \epsilon_0 A}{d} \tag{2}$$

with  $\kappa$  is the relative permittivity of the material,  $\epsilon_0$  is the vacuum permittivity (8.854 x 10<sup>-12</sup> F/m), A is the plate area  $(m^2)$ , and d is the distance between the plates (m). In a vaccum the  $\kappa$  value is 1, in air, the  $\kappa$  value is 1.0006, in water, the  $\kappa$  value is 78.5, in ethanol, the value is 24.3 and in methanol is 32.6. Therefore, if the vacuum (or air) is used as the reference capacitance, the capacitance of a material can be expressed as shown in (3), i.e.,

$$C = \kappa C_0. \tag{3}$$

In this study, ethanol, methanol, or their mixtures were used as dielectric materials to modify C. During the experiment, ethanol-methanol at room temperature (25°C) was heated in the CSMS equipped with a heater, raising its temperature to 43°C. The ethanol-methanol evaporates, causing C to change. The hypothesis assume that the capacitance C is proportional to the material quantity, and its rate of change follows a power law with time,  $rt^b$ . When all ethanol-methanol evaporates, the capacitance reaches  $C_s$ . Thus, the rate of change of capacitance is given by:  $\frac{d\mathcal{C}}{dt} = -rt^b(\mathcal{C}-\mathcal{C}_s).$ 

$$\frac{dC}{dt} = -rt^b(C - C_s). \tag{4}$$

This equation can be modified by introducing an effective time parameter to shift the peak time of the capacitance change, resulting in the following:

$$C = \begin{cases} C_s, & t \le t_a \\ C_s + (C - C_s) \exp\left(-\frac{r}{b+1}(t - t_a)^{b+1}\right), & t > t_a \end{cases}$$
 (6)

Fig. 1 and Fig. 2 illustrate the function in (6) for some given parameters.

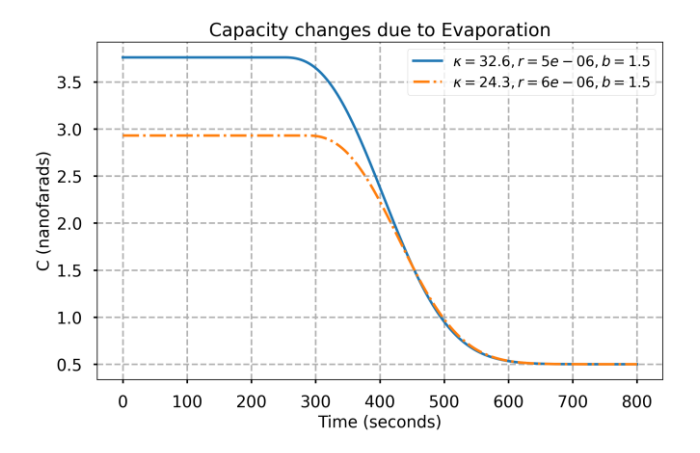


Fig 1. The simulation of capacitance variation due to evaporation for two different materials was conducted in accordance with (6). Each material has an initial capacitance value of  $32.6C_{ref} + C_s$  and  $24.3C_{ref} + C_s$ ,

where  $C_s = 5C_{ref}$  represents the capacitance of the device without external material, and  $C_{ref} = 0.1 \, nf$  serves as the reference capacitance.

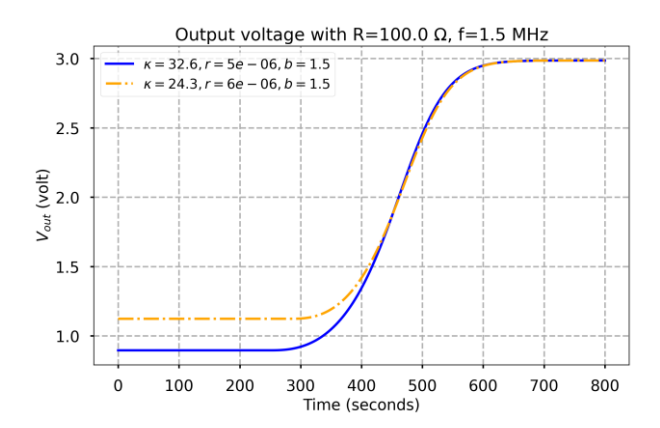


Fig 2. Simulation of CSMS output voltage with a 3.3-Volt power supply and internal resistor R=100 ohm according to (1) and (6).

Additionally, a classical linear evaporation model is frequently used to describe sessile or suspended droplet behavior, where the squared droplet diameter decreases linearly with time according to :  $\left(\frac{d}{d_0}\right)^2 = -rt$ 

$$\left(\frac{d}{d_0}\right)^2 = -rt\tag{7}$$

In this equation, d represents the instantaneous droplet diameter at time t, and  $d_0$  is the initial diameter of the droplet at the beginning of the evaporation process. The parameter rdenotes the evaporation rate constant (in s<sup>-1</sup>), which quantifies the rate at which the squared diameter decreases due to mass loss. Finally, t is the elapsed time (in seconds). In one study, this model was applied to a 92% ethanol droplet at 24 °C, and the evaporation rate constant was reported as  $r = 0.001111 \text{ s}^{-1}$  [3]. While this approach provides a good approximation for diffusion-limited evaporation under isothermal conditions, it does not capture the nonlinear characteristics observed in this study under heating and binary composition effects. Nonetheless, it offers a valuable reference point to compare the effective evaporation dynamics derived from the capacitance response.

#### C. Regularization

Regularization techniques in classical regression penalization parameters, including Ridge  $(L_2)$ , Lasso  $(L_1)$ , or Elastic Net (combination of  $L_1$  and  $L_2$  penalties) [11]. Least Absolute Shrinkage and Selection Operator (Lasso) performs feature selection by adding the absolute sum of coefficients as a penalty, simplifying the model to include only the most significant features. Ridge adds the squared sum of coefficients as a penalty, stabilizing coefficients even in the presence of multicollinearity. Ridge effectively reduces overfitting without feature selection. Elastic Net combines Elastic Net combines  $L_1$  and  $L_2$  penalties, enabling feature selection like Lasso while stabilizing coefficients and mitigating overfitting like Ridge. Additionally, cross validation is a robust approach to split datasets into subsets for model training and validation, ensures better generalization and reduce overfitting, especially when the data is limited [11].

# D. Partial Least Squares Regression

Partial Least Squares Regression (PLSR) is a multivariate regression method to form linear relationship between response variables (Y) and predictor variables (X). Operation of PLSR is used by bulding the linear combination from the predictor variables (X), thereby effectively managing multicollinearity by identifying the most correlated X variables with Y variables [1]. PLSR mostly used for spectral data, such as in quantifying methanol and ethanol content in wine using FTIR [12]. PLSR also used for complex data like artificial intelligence with 36 predictor variables [13]. PLSR capability to handle complex data make it ideal to analyze time series data from sensor reading, where strong correlations often exist between data points, as is the case with ethanol-methanol mixtures evaporation over time. Furthermore, by its latent variables, PLSR can identify smooth patterns within the data that might not be seen with univariate regression methods.

# E. Deep Learning

Both deep learning and ANN can perform classification or regression predictions. They are applicable in tasks such as image and voice recognition, natural language processing, and predictive modeling [14]. Neural Networks (NN) consist of layers or interconnected nodes or usually called by neurons that used to model complex pattens and relationships in data. They can be applied to various tasks, including image and voice recognition, natural language processing, and predictive modeling. NN has become an integral part of the study and application of machine learning. A explained previously, NN can be used for predictions in classification and regression [15]. In classification, NN creates a model that can classify data into different categories. During the training process, predefined inputs and outputs used to adjust the weights and biases in every neurons in the network [16]. For regression, NN us used to predict continuous values. Regression in NN is a classification in NN with a single class. In regression, NN's output generates a continuous value, such as temperature, humidity levels, or stock prices [17].

Several steps must be considered to design NN for classification, from selecting the appropriate type of NN for the problem to be solved, such as Multi-Layer Perceptron (MLP), Convolutional Neural Network (CNN), or Recurrent Neural Network (RNN). After that, configure the number of neurons and layers, choose the activation function, set the regularization level, train the NN methods, and finally evaluating the prediction results [18]. Common activation functions used in classification are sigmoid, tangent hyperbolic, or ReLU [19]. Meanwhile, commonly used optimization algorithms include gradient descent, stochastic gradient descent, or Adam [20].

# F. Artificial Neural Networks (ANN)

Artificial Neural Networks (ANN) are utilized to predict material compositions based on parameters, for example, as shown by [21]. Here, mango peel, rich in antioxidants and other bioactive compounds, was studied using microwave-assisted extraction and Response Surface Methodology (RSM) alongside ANN. Variables like extraction time, solvent-to-plant ratio, and ethanol concentration significantly influenced total phenol compounds (TPC) and antioxidant

activity (TEAC) in extracts from Tommy and Sugar mango peel varieties. The ANN has been used to develop predictive models for the compressive strength of rubberized concrete, incorporating features such as rubber size, percentage of rubber replacement for natural aggregates, cement content, water content, fine aggregate content, coarse aggregate content, and curing time[22]. The other author used ANN to predict the density and heat capacity of ionic liquid (IL)water binary systems, addressing the high viscosity and synthesis cost of ILs[23]. The ANN model, XGBoost, and LightGBM were applied using features such as system components and substituents on the cation. ANN can predict surface tension and viscosity using some chemical and physical properties as the features. In those examples, the authors used standard ANN as the architecture [24]. In this paper, a new layer of neural networks is introduced. A typical ANN is structured as a composition of activation functions applied to linear functions. The mathematical form of a layer of ANN is

$$z_L = f_L(z_{L-1} \cdot W_L + b_L) \tag{8}$$

The input layer needs  $z_0$ =X as the input. Here,  $f_L$  is the activation function of the layer-L. Usually "relu" is chosen for the activation functions of the internal layers. For nonlinear regression, the last layer has no activation layer (or  $f_L(x) = x$ ).  $W_L$  and  $b_L$  are the weights and biases of layer-L.

# III. METHOD

# A. Instrument preparation

The research process is summarized in the flowchart shown in Fig. 3.

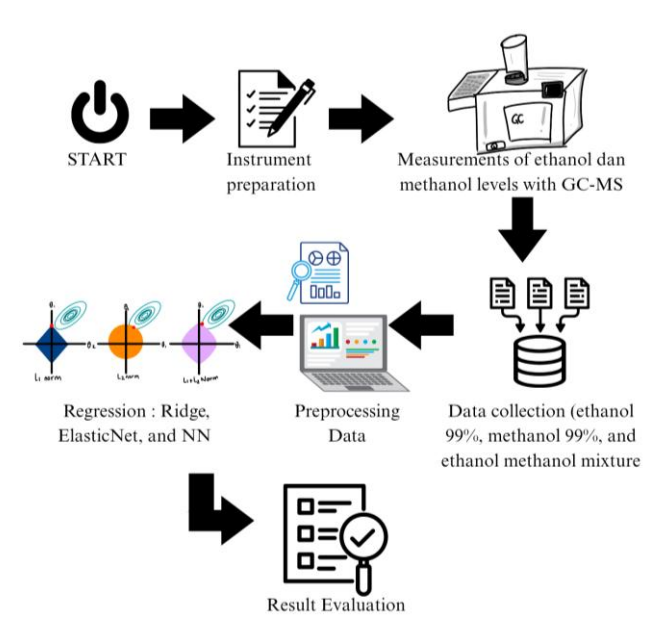


Fig 3. Flowchart of research steps

The CSMS was modified by adding a heater and a ring at the top to ensure the sample droplets remained localized. A single CSMS was connected to the A0 pin of the ESP8266 microcontroller. The heater was constructed using nichrome wire powered by 5V and positioned beneath the CSMS. This modification ensured that the heater operated as a solenoid without contacting the sensor's electrodes. The electrodes of

the CSMS were shortened to prevent direct contact with the heater (Figure 4).

### B. Measurement Design

The evaporation of an ethanol-methanol mixture is indirectly assessed using a modified Capacitive Soil Moisture Sensor (CSMS) V2.0 paired with an ESP8266 microcontroller. Approximately 10 drops of the ethanol-methanol mixture typically induce a 0.6 Volt deviation from its initial empty state. The CSMS includes a custom-made heater powered by a 5 Volt supply, constructed from a 3.5 cm length of nichrome wire with a resistance of 14 ohms at room temperature, configured as a solenoid. The CSMS output connects to the ESP8266's A0 pin as an analog input, operating at 3.3 volts.





Fig 4. The modified CSMS includes a heater (red) and an O-ring (blue). The original electrode needs to be shortened to accommodate the heater, ensuring that the heater has no contact with the electrodes.

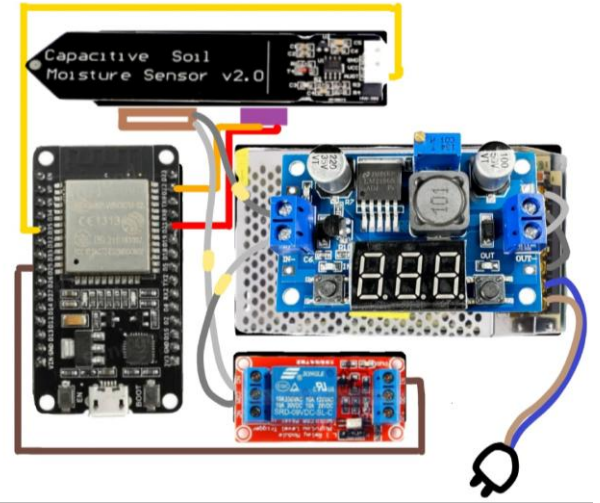


Fig 5. Sketch of tools used in the research

The heater provides a stable temperature under a constant voltage. In this setup, applying 5.12 volts raises the temperature from room temperature to an asymptotically stable 43°C. The final temperature is influenced by environmental conditions; however, incorporating a temperature regulator into the circuit can ensure consistent temperature control. A rubber O-ring with a radius of 1.0 cm is installed on the CSMS electrode, designating it as the designated area for depositing the ethanol-methanol mixture. The ethanol-methanol mixture should pour a volume of 0.7 milliliters (or approximately 10 drops) into the O-ring. A BME280 temperature sensor is attached beneath the O-ring, allowing it to measure the actual temperature in the area where the liquid drops are deposited. In addition to

temperature, the BME280 sensor also measures air humidity and atmospheric pressure.

# C. Measurement of Methanol and Ethanol Levels with GC-MS

Ethanol and methanol concentrations were validated using GC-MS in a standardized laboratory to ensure the purity of the 99% ethanol and methanol used in the experiments. The results included the area response and concentrations as indicated by the chromatograms obtained from the GC-MS analysis.

#### D. Data Collection

A dropper was used to dispense precisely 10 drops (approximately 0.70 mL) of the ethanol-methanol mixture into the ring-shaped container of the CSMS. The measurement procedure is as follows:

- 1. Start the heater and wait until the BME280 sensor indicates a stable temperature of around 43°C.
- Begin continuous data acquisition at one-second intervals.
- 3. Pour a 0.7 milliliter sample of ethanol-methanol into the O-ring.
- 4. Record data for 600 seconds (10 minutes) for each sample

The heater remains active throughout, ensuring the temperature remains constant even as samples are replaced.

The samples of ethanol-methanol mixture are labeled as the fraction of ethanol in the mixture, i.e., 1.0, 0.8, 0.6, 0.4, 0.2, 0.0. For example, label 0.6 consists of 60% ethanol and 40% methanol. The label 1.0 is the approximation of the real concentration of pure ethanol, which is only 0.96 according to the gas chromatography (GC) measurement. On the other hand, the label 0.0 is related to the approximation of pure methanol, i.e., 0.97 according to GC. The labels 0.2, 0.4, 0.6, and 0.8 are associated with the ratio of those pure solvents.

# 1) Preprocessing Data

Preprocessing steps included central-shifting, padding, and smoothing to refine the evaporation time series data for regression analysis. Central-shifting aligned curves in the time domain by shifting them to overlap based on the median time when drastic evaporation occurred. Padding added values at the beginning and end of measurements with varying lengths, standardizing the time series for consistent sample duration. Average smoothing was applied to reduce noise in the evaporation curves. This method smoothed the data by calculating the average of several data points around each point to create a more regular curve.

# 2) Regression Method with Ridge, Elastic Net, and NN

Regression modeling was performed using various methods, employing features derived from the preprocessed raw data. Specific feature points were selected by Gaussian distribution or with Elastic Net and Ridge regularization. Additionally, the results were analyzed using Artificial Neural Networks (ANNs) with multiple layers, as well as hybrid approaches sucah as ANN-Ridge and ANN-Elastic Net. Descriptive statistics were also Descriptive statistics were also incorporated as features in conuction with ANNs for further analysis.

Representative points were choosen from 800 sampled points in the original dataset for feature selection from the raw signals, guided by the Gaussian distribution. These pounts wew concentrated aroung the steeoest portion of the evaporation curve. The time range was constrained between 0.0 to 0.80 to simplify the range and avoid excessive complexity. A subset of n points was selected to reduce the number of features, thus minimizing model complexity. For example, 55 and 35 feature points were selected for Ridge regression using Gaussian-distributed representative points. The selected features for each sample were divided into 70% training data and 30% testing data. Regression modeling based on concentrations was performed using Ridge and Elastic Net penalties, with varying alpha values to determine the strength of regularization. Features selected through Elastic Net were prioritized and filtered based on their importance, followed by an evaluation of model performance using coefficients of determination  $(R^2)$ , Mean Squared Error (MSE), Root Mean Squared Error (RMSE), RMSE standardized by standard deviation (RMSE/SD), Mean Absolute Error (MAE), and MAE standardized by standard deviation (MAE/SD).

Tests were also conducted using ANNs combined with Ridge and Elastic Net, varying the number of neurons per layer based on the feature selection results from Elastic Net. Additionally, ANN models incorporating seven statistical features (Stat-ANN) were tested. These statistical features included mean, standard deviation, minimum, maximum, range, skewness, and kurtosis. The formulas for standard deviation, mean, skewness and kurtosis were calculated using equations (9) to (12).

$$SD = \sqrt{\frac{1}{n} \sum_{i=1}^{n} (x_i - \bar{x})^2}$$

$$\bar{x} = \frac{1}{n} \sum_{i=1}^{n} x_i.$$
(9)
(10)

$$\bar{x} = \frac{1}{n} \sum_{i=1}^{n} x_{i}$$
 (10)  
Skewness =  $\frac{n}{(n-1)(n-2)} \sum_{i=1}^{n} \left(\frac{x_{i} - \bar{x}}{SD}\right)^{3}$  (11)

Kurtosis =

$$\frac{n(n+1)}{(n-1)(n-2)(n-3)} \sum_{i=1}^{n} \left(\frac{x_i - \bar{x}}{SD}\right)^4 - \frac{3(n-1)^2}{(n-2)(n-3)}$$
(12)

Here, n represents the total number of data points,  $x_i$  denotes an individual data value,  $\bar{x}$  is the mean, and SD is the standard deviation [25]. Descriptive statistics were employed to capture the unique characteristics of each alcohol concentration.

The training results for each model—classic methods like Ridge and Elastic Net, ANN with varying neuron layers, ANN-Elastic Net hybrids, and Stat-ANN—were compared based on model performance metrics. These included the coefficient of determination ( $R^2$ ), Mean Squared Error (MSE), Root Mean Squared Error (RMSE), RMSE/SD, Mean Absolute Error (MAE), and MAE/SD.

The goodness-of-fit metrics for Ridge, Elastic Net, and ANN models included performance indicators such as determination coefficient, MSE, RMSE, RMSE/SD, MAE, and MAE/SD. For Elastic Net models, modifications to the  $L_1:L_2$  ratio were tested to optimize model performance. This comprehensive approach ensured robust model performance, with each method tailored to effectively analyze and predict ethanol-methanol mixtures.

### IV. RESULT AND DISCUSSION

Dropping ethanol-methanol into the CSMS O-ring is highly susceptible to human error. Therefore, the X(t) data recorded for each sample needs to be time-shifted so that the median value of X(t) aligns with the center of the time domain. This shift must be followed by padding to ensure uniform sample length. Data smoothing can be performed using averaging techniques. Example results are illustrated in Fig. (6).

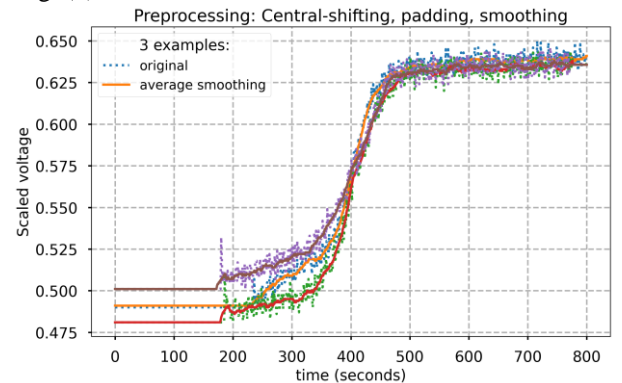


Fig 6. Curves from Example Preprocessing Data Result by: centralshifting, padding, smoothing

The preprocessing process revealed that each sample curve exhibited three distinct phases: a gradual increase during the initial stage of evaporation, a steep rise in the mid-phase, and a plateau at the final stage. The initial gradual increase reflects minimal evaporation as the sample absorbs heat energy. The mid-phase is marked by a significant increase in evaporation, driven by molecules gaining sufficient energy to transition into the gaseous phase. The final plateau occurs due to the reduced liquid volume, limiting further evaporation. This trend is consistent with findings by [26], which highlight that before the steep evaporation phase, minimal evaporation occurs as molecules absorb heat, while at the end, the trend flattens due to the diminished liquid volume.

The results revealed an S-shaped evaporation curve across all samples, beginning with an initial increase, followed by a rapid rise, and finally a decline. This pattern aligns with the description provided by (1). Additionally, it is consistent with the equation relating voltage to capacitance. As capacitance increases, the voltage decreases. Therefore, the initial liquid with specific capacitance produces a very low output, as observed in the samples (Fig. 6). The high initial capacitance (low voltage output) is due to the dielectric material enhancing the capacitor's ability to store charge. The capacitance decreases as evaporation progresses, reducing the liquid material and rapidly increasing voltage in accordance with the exponential function described in (6).

Several methods can be used to perform non-linear regression on data in Fig. 6. Firstly, the data is resampled at specific time points  $t_j$ , where j does not need to be chosen linearly. Resampling is necessary to reduce the number of data points compared to the number of samples. To prevent overfitting, it is important to choose M < N. Consequently, data X will have dimensions  $N \times M$ , where N represents the number of samples, and M represents the number of time

samples, which are treated as features. The method can be addressed using classical regression techniques like Ridge, Elastic-net, or modern approaches such as ANN. This is in accordance with the statement that the number of features should not exceed the number of samples because the more features there are, the greater the tendency for overfitting to occur[27].

The dataset comprises 88 samples, each containing 800 data points. Prior to performing regression analysis, the data undergo resampling. In this process, a Gaussian function is employed to select points, resulting in non-uniform intervals. These intervals are denser near the center of the sample data. The configuration of the selected time coordinates is depicted in Fig. (7).

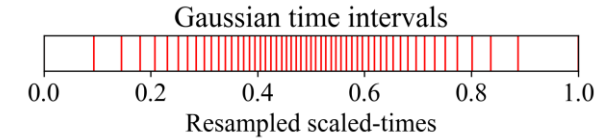


Fig 7. Time Coordinates Selected by Gaussian Method

In Fig. (7), the original time domain 0-800 seconds is scaled into 0-1, and then 55 selected points are utilized for the regression analysis instead of the original 800 points. Consequently, the data has a shape of  $88 \times 55$ , which can be split into training and test sets. The training set comprises 70% of the data (61 x 55), while the test set comprises 30% (27 x 55).

Partial Least Squares Regression (PLSR) was initially employed as a baseline method to evaluate the predictive capability of the capacitance-derived feature set. Given the structure of the dataset (88 samples, 55 selected time features), PLSR is particularly advantageous due to its ability to handle multicollinearity and extract latent variables that best explain the variance in both predictors and response variables. This is especially relevant in high-dimensional problems, where the number of features approaches or exceeds the number of samples.

To determine the optimal number of latent components, models were trained and evaluated with varying component counts from 10 to 50, using an 80:20 train-test split. The model performance stabilized around 30 components, where the additional latent dimensions did not significantly improve the prediction.

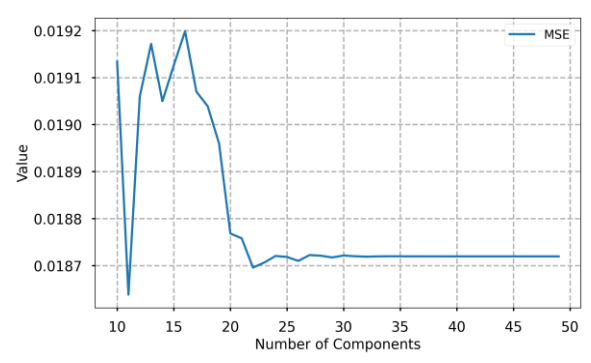


Fig. 8. MSE Value in Every Components Result

At the optimal setting (30 n components), PLSR achieved 0.01872 for Mean Squared Error (MSE), 0.1368 for Root Mean Squared Error (RMSE), 0.3457 for

RMSE/SD, and 0.8805 for Coefficient of Determination (R<sup>2</sup>).

These results demonstrate that the model could explain approximately 88% of the variance in ethanol—methanol concentrations. The RMSE/SD value < 1 confirms that the prediction error is notably smaller than the inherent variability of the target data. While PLSR effectively handled the high-dimensional dataset (800 features with only 88 samples), it required a relatively large number of latent components, up to 30 to achieve this level of performance. This indicates that although the model works well, its complexity remains considerable.

To reduce model complexity and the number of required features, further analyses were carried out using alternative regression methods. Methods such as ridge and elastic net regression were explored because they offer feature reduction through regularization, potentially decreasing the number of predictors to fewer than the number of samples. Additionally, these techniques provide more interpretable models and are less prone to overfitting when the feature count is minimized.

The ridge regression analysis produces various results depending on the ridge parameter alpha, as shown in Table 1. According to the table, the optimal result (lowest RMSE) is obtained with an alpha value of 0.001, using 55 points as the number of features. In addition to using 55 points, 35 points were also used as features in the same way as selecting 55 points. According to Table 1, the reduction of the number of features changes slightly the RMSE, MAE, and R<sup>2</sup>.

Table 1. 55 or 35 points is used as the features of Ridge-Regression.

HERE THE STANDARD DEVIATION OF TEST-DATA IS 0.3 /9							
Alpha	RMSE		MAE	MAE		RMSE/SD	
	55	35	55	35	55	35	
0.000	0.249	0.213	0.206	0.162	0.658	0.562	
	6	0	4	5	5	1	
0.001	0.119	0.120	0.081	0.082	0.315	0.316	
	6	0	9	1	6	6	
0.010	0.128	0.129	0.093	0.094	0.340	0.341	
	9	6	2	0	1	8	
0.100	0.156	0.161	0.119	0.123	0.412	0.424	
	5	0	2	8	9	8	
0.500	0.231	0.244	0.198	0.211	0.610	0.643	
	4	0	5	6	5	8	
1.000	0.277	0.289	0.244	0.256	0.731	0.763	
	4	4	4	0	9	4	

MAE/S	D	$\mathbb{R}^2$	
55	35	55	35
0.544	0.428	0.566	0.684
5	8	3	1
0.216	0.216	0.900	0.899
2	5	4	7
0.245	0.248	0.884	0.883
9	1	3	2
0.314	0.326	0.829	0.819
4	7	5	6
0.523	0.558	0.627	0.585
7	3	3	6
0.644	0.675	0.464	0.417
9	4	3	2

Reducing the number of features to 35 slightly decreases the model's predictive power compared to 55 features, the performance degradation is minimal. These findings suggest that a more compact feature set can still provide high accuracy while reducing computational cost and risk of overfitting. Accuracy and parsimony balance is important to future model deployment and hardware constrained environments.

To further investigate the relevance of the selected time coordinates and to identify which features contribute most to prediction, Elastic Net regression was employed. Using the 55 selected points, the number of features (nf) those have nonzero values of Elastic Net coefficients was counted (Table 2), providing deeper insight into feature importance and potential for dimensionality reduction.

TABLE 2. MODEL PERFORMANCE OF ELASTIC NET BASED ON VARIATIONS

IN ALPHA, FEATURES, AND L1/L2 RATIOS

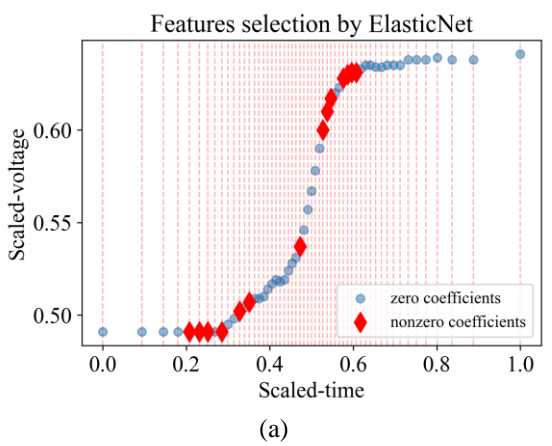
	- 11	, , that in i, i	Litteren	, TIND EITE	2 10 11105		
Alpha	$L_1$	RMSE	MAE	RMSE	MAE/	$\mathbb{R}^2$	nf
	Ratio			/ SD	SD		
0.006	0.001	0.208	0.173	0.5487	0.457	0.699	5
		0	5		7	0	5
0.000	0.238	0.120	0.082	0.3177	0.218	0.899	4
		4	9		8	1	1
0.000	0.475	0.120	0.082	0.3179	0.216	0.899	3
		5	2		9	0	4
0.000	0.713	0.121	0.082	0.3206	0.218	0.897	2
		5	7		2	2	2
0.000	0.948	0.124	0.084	0.3291	0.222	0.891	1
		7	5		9	7	0
0.000	0.956	0.124	0.084	0.3292	0.222	0.891	1
		8	5		8	6	0
0.000	0.964	0.124	0.084	0.3294	0.222	0.891	9
		9	4		8	5	
0.000	0.972	0.125	0.084	0.3297	0.222	0.891	9
		0	5		9	3	

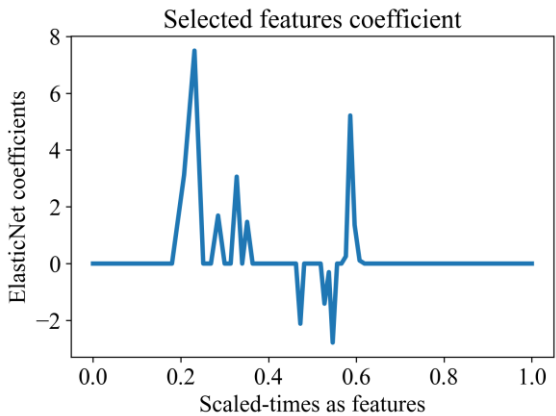
The model performance metrics showed no significant differences in RMSE, MAE, RMSE/SD, MAE/SD, and  $R^2$  except when using 55 features, which resulted in the lowest  $R^2$  value and the highest errors among all cases. Table 1. indicates that most alpha values in Elastic Net regression were close to 0.000. However, the results and feature selection were still influenced by an increase in the  $L_1$  ratio, which eliminated less impactful features and thus influenced the outcomes. In Elastic Net, the  $L_1$  ratio determines the number of retained features; a higher  $L_1$  ratio reduces the selected features, leaving only 9 features out of 55, with results comparable to using 41 features. Fewer features reduce the likelihood of overfitting, indicating that 9 features are sufficient to model the samples using Elastic Net regression.

At  $L_1$  ratios of 0.972 and 0.964 with 9 features, the results were similar, but the 0.964 ratio provided slightly better performance. Thus, the  $L_1$  ratio of 0.964 with 9 features was deemed optimal, as it achieved low error values and a high coefficient of determination (approaching 1.0) without significant deviation from the results obtained with more features and higher  $L_1$  ratios. An example of feature selection using Elastic Net is shown in Fig. (9). The feature selection results from Elastic Net are depicted in Fig. 8(a), where selected coefficients are marked with red diamonds, while other coefficients with zero values are shown in gray. Additionally, Fig. 9(b) highlights several peaks among the selected coefficients, indicating higher values that represent the most significant features for prediction.

Using Elastic Net regression with 9 features, it was determined that only 9 distinguishing points were necessary to differentiate one sample type from another. These 9 feature points, based on time, also demonstrated that the median value during the rapid evaporation phase did not

indicate critical points, as previously hypothesized in Ridge regression. Fig. 9(b) shows the Elastic Net coefficient points, with 9 peaks, where higher peak values signify a greater influence of the feature on prediction outcomes. Overall, Elastic Net results demonstrated that the 9 features sufficiently distinguished the sample types. Among the selected points, those occurring just before the steep evaporation phase and at the transition between steep and plateau phases were identified as critical for distinguishing one alcohol mixture from another. These points differentiate samples due to the ethanol-methanol mixture's unique evaporation characteristics when reaching the liquid-gas equilibrium, varying between concentrations. This behavior is influenced by the azeotropic interactions between ethanol and methanol, which alter the component relationships and evaporation patterns based on the concentration [28].





(b)
Fig. 9. Results of feature selection with 9 features and Elastic Net coefficients

In addition to Ridge and Elastic Net, several other methods were employed to determine the best modeling approach for predicting sample concentrations. These included simple ANN, ANN with  $L_1$  or  $L_2$  regularization (ElNet-ANN), and ANN using statistical feature values from the data with varying neuron counts in the ANN layers. A comparative analysis of the methods used is presented in Table 3.

TABLE 3. COMPARISON OF MODEL PERFORMANCE ACROSS DIFFERENT

METHODS						
Method	Alpha	$L_1$	RMSE	MAE	RMSE	
		Ratio			/ SD	
Elastic Net	0.000	0.238	0.1204	0.0829	0.3177	

(32,16,1) Stat-ANN (32,16,1)	-	-	0.0912	0.0725	0.2406
ANN	2.5810	0.90	0.0720	0.0555	0.1921
(32,16,1) <b>ElNet-</b>	2.3x10 <sup>-5</sup>	0.90	0.0728	0.0533	0.1921
(32,16,1) ElNet-ANN	0.000	0.97	0.1065	0.0842	0.2809
(16,8,1) ANN	-	-	0.0854	0.0597	0.2253
(32,16,1) ANN	-	-	0.0881	0.0674	0.2324
(64,16,1) ANN	-	-	0.0810	0.0576	0.2137
ANN	-	-	0.0855	0.0597	0.2257
Ridge	0.001	-	0.1200	0.0821	0.3166
Ridge	0.001	-	0.1196	0.0819	0.3156
	0.000	0.964	0.1249	0.0844	0.3294
	0.000	0.475	0.1205	0.0822	0.3179

MAE / SD	$\mathbb{R}^2$	nf
0.2188	0.8991	41
0.2169	0.8990	34
0.2228	0.8915	9
0.2162	0.9004	55
0.2165	0.8997	35
0.1575	0.9491	55
0.1520	0.9543	55
0.1779	0.9460	55
0.1575	0.9492	35
0.2222	0.9211	9
0.1405	0.9631	14
0.1912	0.9421	7

Based on the comparison of methods, all approaches yielded RMSE/SD and MAE/SD values below 1.0. These indicate that each model successfully captured the primary patterns in the data, as the model errors were smaller than the natural variation in the data.

The results in Table 3 show that the Elastic Net-ANN method with 14 feature points and a 3-layer architecture (with 32, 16, and 1 neurons in each layer, respectively) achieved the highest coefficient of determination ( $R^2$ ) of 0.9631 This indicates that the model performed exceptionally well in regression (approaching 1.0) with relatively low error values, specifically RMSE of 0.0728 and MAE of 0.0533. Elastic Net-ANN with only 9 features also yielded a relatively high  $R^2$  of 0.9211. However, increasing the feature count to 14 significantly improved the coefficient of determination. While adding more feature points enhances the model's ability to represent the evaporation patterns, excessive features may lead to overfitting, as the model becomes overly tailored to the training data compared to the test data.

The next-best performance was observed with an  $R^2$  of 0.94 for a 3-layer ANN using 55 features, with neuron counts of 32, 16, and 1 in each layer. Similarly, an  $R^2$  of approximately 0.94 was achieved with a 3-layer ANN using 35 features, with neuron counts of 36, 16, and 1. Additionally, Stat-ANN with only 7 statistical features (minimum value, maximum value, standard deviation, skewness, kurtosis, range, and mean) and a 4-layer ANN architecture (32, 16, 16, and 1 neurons) achieved an  $R^2$  of Although several methods achieved coefficients of determination ( $R^2 > 0.94$ ) and model errors smaller than data variability (based on RMSE/SD and MAE/SD), models with fewer features were generally preferred due to the limited dataset and to avoid overfitting. As the number of features increases, the risk of overfitting also grows. Therefore, the Stat-ANN model with an  $R^2$  of 0.9421 and a correlation coefficient of 0.9706 was deemed sufficient to model the data using only 7 features. Stat-ANN provided a reliable model with a simple approach, summarizing the dataset effectively and reducing overfitting risks compared to more complex models such as Elastic Net-ANN or ANN with 55 or 35 features. This aligns with the statement that simpler models are more resistant to overfitting compared to more complex ones.

Based on the comparison of model performance, the Elastic Net model with 14 features and the Stat-ANN model with 7 features were identified as the two best-performing models. Both models used relatively few features while achieving high  $R^2$  values exceeding 0.94. However, the Stat-ANN model with 7 features and a simpler architecture (4 layers with 32, 16, 16, and 1 neurons, respectively) was determined to be sufficient for predicting ethanol-methanol mixture concentrations.

In addition to the concentration prediction models, the present study also investigates the evaporation dynamics of ethanol—methanol mixtures using a nonlinear modeling approach. The model is expressed as:

$$m(t) = \exp(-r(t-t_a)^{b+1}), t > t_a$$
 (13)

Where m(t) is the normalized material quantity at time t, r is the evaporation rate constant, b is the exponent describing the curvature of the decay, and  $t_a$  is the activation time or the onset of significant evaporation. This formulation allows the modeling of a dynamic, time-shifted evaporation process, capturing the nonlinearity commonly observed in real binary volatile systems. From this model, an effective evaporation rate  $r_e$  can be derived as:

$$r_e = r\tau^b m(\tau)/m_0 \tag{14}$$

Where  $\tau = t - t_a$  is the effective duration after activation and  $m_0$  is the initial material quantity (before evaporation begins). A sample fit of the nonlinear model to experimental capacitance-derived data is shown in Fig. 9, highlighting the ability of the model to match the observed evaporation profile.

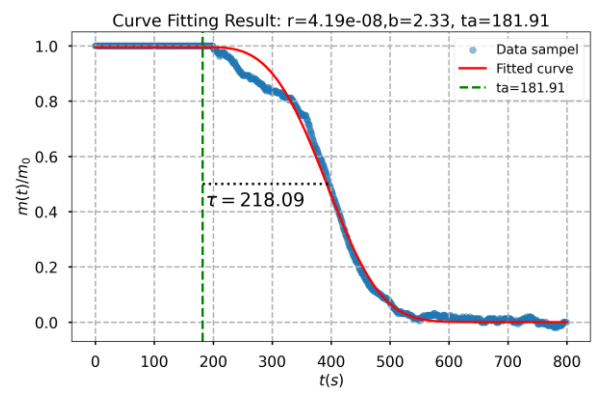


Fig. 10. Curve Fitting Result for Nonlinear Model

To facilitate comparison with more conventional evaporation models, the nonlinear profile was also approximated using a linear fit at the point of maximum evaporation (e.g., at t=400s), yielding an estimated linear evaporation rate constant  $r_l$ . These values of  $r_e$  and  $r_l$  are summarized in Table 4., across different methanol fractions (Y) in the ethanol–methanol mixtures with pure ethanol as 0.00 and pure methanol written as 0.99.

Table 4. Values of  $r_e$  and  $r_l$  in different concentration of ethanol-

METHANOL MIXTURES						
Y	$r_e$	SD(r <sub>e</sub> )	$r_l$	$\mathrm{SD}(r_l)$		
0.00	0.0093	0.0013	0.0025	0.0003		
0.20	0.0067	0.0008	0.0016	0.0002		
0.40	0.0065	0.0004	0.0015	0.0001		
0.60	0.0066	0.0004	0.0014	0.0001		
0.80	0.0063	0.0006	0.0013	0.0002		
0.99	0.0065	0.0007	0.0015	0.0001		

The results show that the effective rate  $r_e$  is consistently higher than the linear approximation  $r_l$ , indicating that the actual evaporation process is more dynamic than what a constant rate model can capture. Notably, the trend in  $r_e$  also aligns with prior experimental findings such as those reported by Sterlyagov (2018), validating the measurement approach and supporting the adoption of a nonlinear framework. This nonlinear modeling method enhances interpretability and flexibility, providing a more realistic representation of evaporation behavior in heated volatile binary systems, which has not been extensively addressed in previous linear evaporation models.

If linear approach is used, the derived evaporation rate  $(r_l)$ is close to 0.001, as expected and in accordance with the previous findings reported by Sterlyagov (2018). In this study, a nonlinear modelling approach was also adopted to capture the S-shaped behavior of the evaporation process more accurately, accounting for the time shifts and concentration dependence. Moreover, the results of the nonlinear effective rate  $(r_e)$  are also close to 0.001, showing that both modeling strategies, despite their different complexities yield comparable outcomes. This similarity indicates that both approaches are valid and capable of describing ethanol-methanol evaporation under moderate heating conditions. However, it should be noted that evaporation rates derived from the models can be influenced by various factors, such as ambient humidity [29], temperature fluctuations [30], wind speed, evaporation pan [31], and other environment conditions. Thus, while the models serve as useful approximations, their agreement with prior studies reinforces their reliability and applicability for analyzing volatile binary mixtures.

Overall, the modeling results show that several yielded satisfactory performance, approaches RMSE/SD and MAE/SD values below 1.0, indicating that the prediction errors are smaller than the natural variability of the data. Among these, the Stat-ANN model with only 7 statistical features and a 4-layer architecture (32, 16, 16, 1 neurons) achieved an R2 of 0.9421, making it the most recommended method in this study. Its simplicity and ability to generalize well, even with limited input features, make it suitable for practical implementation. While the results still offer room for improvement and expansion in future work, the Stat-ANN approach provides a strong foundation for accurate and efficient modeling of ethanol-methanol concentration using sensor data.

#### V. CONCLUSION

Ethanol and methanol can be mixed to produce more efficient fuel. The concentration of ethanol and methanol is typically measured using gas chromatography (GC). However, their evaporation characteristics, such as dielectric properties, vary and can be measured using a capacitive soil moisture sensor (CSMS). The CSMS equipped with a

heating element was utilized in this study to accelerate evaporation, operating at a temperature of  $43 \pm 1.5^{\circ}$ C for a measurement duration of 10 minutes. The system demonstrated the ability to determine the ethanol-to-methanol ratio in mixtures through regression models. The most effective approach, based on testing, was the Elastic Net-ANN regression model with 14 features and the Descriptive Statistics-ANN model. Both methods achieved high determination coefficients of 0.9631 and 0.9421, respectively, indicating excellent variability explanation. Furthermore, the models exhibited low and comparable RMSE values for both training and testing datasets, signifying minimal overfitting.

However, the Descriptive Statistics-ANN model with 4 layers is recommended for its simplicity and focus on key data patterns. By utilizing features such as mean, standard deviation, minimum value, maximum value, range, skewness, and kurtosis, this model effectively characterizes sample variations. It achieved a determination coefficients value of 0.9421 and RMSE values of 0.0711 (training) and 0.0912 (testing), further supporting its resistance to overfitting.

Furthermore, the evaporation dynamics were modeled using both linear (d²-law approximation) and nonlinear approaches. Both models yielded effective evaporation rates around 0.001, demonstrating consistency with previous studies. The nonlinear model, however, captured the characteristic S-shaped curve observed in the experimental data more effectively, reflecting the time-shifted and concentration-dependent nature of the evaporation process. This confirms that while the linear model remains a valid and simple approximation, the nonlinear approach offers improved accuracy in describing real evaporation behavior under moderate heating conditions.

Thus, the research demonstrated that PLSR, Ridge Regression, Elastic Net, and Neural Network models effectively captured the relationship between evaporation dynamics and influencing factors. Among these, the Neural Network model exhibited the highest predictive accuracy, indicating its robustness in handling complex nonlinear relationships. The findings highlight the significance of precise modeling techniques for optimizing industrial applications involving volatile mixtures. Future research could explore add additional variables, such as temperature and humidity effects, to further refine the model's predictive capability.

#### REFERENCES

- [1] A. Liu, Y. Song, Z. Xu, X. Meng, and Z. Liu, "Non-destructive Determination of the Soluble Solid Content in Winter Jujubes Using Hyperspectral Technology and the SCARS-PLSR Prediction Model," *IAENG Int. J. Comput. Sci.*, vol. 52, no. 3, pp. 555–565, 2025.
- [2] M. Soori, B. Arezoo, and R. Dastres, "Artificial neural networks in supply chain management, a review," *J. Econ. Technol.*, vol. 1, no. October 2023, pp. 179–196, 2023, doi: 10.1016/j.ject.2023.11.002.
- [3] A. N. Sterlyagov, V. N. Letushko, M. I. Nizovtsev, and V. Y. Borodulin, "Experimental study of the evaporation of suspended droplets of a water-ethanol solution," *J. Phys. Conf. Ser.*, vol. 1128, no. 1, 2018, doi: 10.1088/1742-6596/1128/1/012055.
- [4] A. P. Wibawa, A. B. P. Utama, H. Elmunsyah, U. Pujianto, F. A. Dwiyanto, and L. Hernandez, "Time-series analysis with smoothed Convolutional Neural Network," *J. Big Data*, vol. 9, no. 1, 2022, doi: 10.1186/s40537-022-00599-y.
- [5] K. Basaran, A. Çelikten, and H. Bulut, "A short-term photovoltaic output power forecasting based on ensemble algorithms using hyperparameter optimization," *Electr. Eng.*, no. February, 2024, doi:

- 10.1007/s00202-024-02281-3.
- [6] S. Raghuram, V. Raghavan, D. N. Pope, and G. Gogos, "Two-phase modeling of evaporation characteristics of blended methanol—ethanol droplets," *Int. J. Multiph. Flow*, vol. 52, pp. 46–59, Jun. 2013, doi: 10.1016/J.IJMULTIPHASEFLOW.2012.12.008.
- [7] C. Y. Zhang, N. B. Lin, X. S. Chai, Zhong-Li, and D. G. Barnes, "A rapid method for simultaneously determining ethanol and methanol content in wines by full evaporation headspace gas chromatography," *Food Chem.*, vol. 183, pp. 169–172, Sep. 2015, doi: 10.1016/J.FOODCHEM.2015.03.048.
- [8] K. Li et al., "Accurate identification of methanol and ethanol gasoline types and rapid detection of the alcohol content using effective chemical information," *Talanta*, vol. 274, p. 125961, Jul. 2024, doi: 10.1016/J.TALANTA.2024.125961.
- [9] B. Abdollahipoor, S. A. Shirazi, K. F. Reardon, and B. C. Windom, "Near-azeotropic volatility behavior of hydrous and anhydrous ethanol gasoline mixtures and impact on droplet evaporation dynamics," *Fuel Process. Technol.*, vol. 181, pp. 166–174, Dec. 2018, doi: 10.1016/J.FUPROC.2018.09.019.
- [10] P. Sun et al., "Artificial neural network models for forecasting the combustion and emission characteristics of ethanol/gasoline DFSI engines with combined injection strategy," Case Stud. Therm. Eng., vol. 54, Feb. 2024, doi: 10.1016/J.CSITE.2024.104007.
- [11] A. R. Nur, A. K. Jaya, and S. Siswanto, "Comparative Analysis of Ridge, LASSO, and Elastic Net Regularization Approaches in Handling Multicollinearity for Infant Mortality Data in South Sulawesi," *J. Mat. Stat. dan Komputasi*, vol. 20, no. 2, pp. 311–319, 2023, doi: 10.20956/j.v20i2.31632.
- [12] V. Thanasi, I. Caldeira, L. Santos, J. M. Ricardo-da-Silva, and S. Catarino, "Simultaneous Determination of Ethanol and Methanol in Wines Using FTIR and PLS Regression," *Foods 2024, Vol. 13, Page 2975*, vol. 13, no. 18, p. 2975, Sep. 2024, doi: 10.3390/FOODS13182975.
- [13] J. J. Yang et al., "Prediction for human intelligence using morphometric characteristics of cortical surface: Partial least square analysis," *Neuroscience*, vol. 246, pp. 351–361, Aug. 2013, doi: 10.1016/j.neuroscience.2013.04.051.
- [14] S. Latif et al., "Deep learning for the industrial internet of things (liot): A comprehensive survey of techniques, implementation frameworks, potential applications, and future directions," Sensors, vol. 21, no. 22, p. 7518, Nov. 2021, doi: 10.3390/s21227518.
- [15] M. M. Taye, "Understanding of Machine Learning with Deep Learning: Architectures, Workflow, Applications and Future Directions," *Computers*, vol. 12, no. 5, p. 91, Apr. 2023, doi: 10.3390/computers12050091.
- [16] S. Haykin, Neural Networks and Learning Machines Neural Networks and Learning Machines, vol. 1–3. in Pearson International Edition, vol. 1–3. Pearson, 2018.
- [17] U. S. Shanthamallu and A. Spanias, "Neural Networks and Deep Learning," *Synthesis Lectures on Signal Processing*. Determination Press, pp. 43–57, 2022. doi: 10.1007/978-3-031-03758-0\_5.
- [18] S. Bi et al., "A Survey on Artificial Intelligence Aided Internet-of-Things Technologies in Emerging Smart Libraries," Sensors, vol. 22, no. 8, p. 2991, Apr. 2022, doi: 10.3390/s22082991.
- [19] B. Yegnanarayana, Artificial neural networks for pattern recognition, vol. 19, no. 2. USA: Oxford University Press, Inc., 1994. doi: 10.1007/BF02811896.
- [20] S. Pouyanfar et al., "A survey on deep learning: Algorithms, techniques, and applications," ACM Comput. Surv., vol. 51, no. 5, Sep. 2018, doi: 10.1145/3234150.
- [21] D. Ramírez-Brewer, S. E. Quintana, and L. A. García-Zapateiro, "Modeling and optimization of microwave-assisted extraction of total phenolics content from mango (Mangifera indica) peel using response surface methodology (RSM) and artificial neural networks (ANN)," Food Chem. X, vol. 22, p. 101420, Jun. 2024, doi: 10.1016/J.FOCHX.2024.101420.
- [22] D. K. Ismael Jaf, A. Abdalla, A. S. Mohammed, P. I. Abdulrahman, Rawaz Kurda, and A. A. Mohammed, "Hybrid nonlinear regression model versus MARS, MEP, and ANN to evaluate the effect of the size and content of waste tire rubber on the compressive strength of concrete," *Heliyon*, vol. 10, no. 4, p. e25997, Feb. 2024, doi: 10.1016/J.HELIYON.2024.E25997.
- [23] Y. Fu, X. Liu, J. Gao, Y. Lei, Y. Chen, and X. Zhang, "Machine learning models for the density and heat capacity of ionic liquid water binary mixtures," *Chinese J. Chem. Eng.*, vol. 73, pp. 244–255,

- Sep. 2024, doi: 10.1016/J.CJCHE.2024.04.019.
- [24] Y. Lei, Y. Shu, X. Liu, X. Liu, X. Wu, and Y. Chen, "Predictive modeling on the surface tension and viscosity of ionic liquid-organic solvent mixtures via machine learning," *J. Taiwan Inst. Chem. Eng.*, vol. 151, p. 105140, Oct. 2023, doi: 10.1016/J.JTICE.2023.105140.
- [25] M. J. Blanca, J. Arnau, D. López-Montiel, R. Bono, and R. Bendayan, "Skewness and kurtosis in real data samples," *Methodology*, vol. 9, no. 2, pp. 78–84, 2013, doi: 10.1027/1614-2241/a000057.
- [26] G. Y. Qiu and J. Ben-Asher, "Experimental Determination of Soil Evaporation Stages with Soil Surface Temperature," Soil Sci. Soc. Am. J., vol. 74, no. 1, pp. 13–22, Jan. 2010, doi: 10.2136/SSSAJ2008.0135.
- [27] J. Subramanian and R. Simon, "Overfitting in prediction models Is it a problem only in high dimensions?," *Contemp. Clin. Trials*, vol. 36, no. 2, pp. 636–641, Nov. 2013, doi: 10.1016/J.CCT.2013.06.011.
- [28] G. M. Fioroni, E. Christensen, L. Fouts, and R. McCormick, "Heat of Vaporization and Species Evolution during Gasoline Evaporation Measured by DSC/TGA/MS for Blends of C1 to C4 Alcohols in Commercial Gasoline Blendstocks," SAE Tech. Pap., vol. 2019-Janua, no. January, pp. 17–19, 2019, doi: 10.4271/2019-01-0014.
- [29] A. N. Sterlyagov, M. I. Nizovtsev, and V. N. Letushko, "Experimental study of evaporation of droplets of water ethanol solution at high relative air humidity," *J. Phys. Conf. Ser.*, vol. 2057, no. 1, 2021, doi: 10.1088/1742-6596/2057/1/012059.
- [30] A. J. Cunliffe, R. Wang, J. Redfern, J. Verran, and D. Ian Wilson, "Effect of environmental factors on the kinetics of evaporation of droplets containing bacteria or viruses on different surfaces," *J. Food Eng.*, vol. 336, no. June 2022, p. 111195, 2023, doi: 10.1016/j.jfoodeng.2022.111195.
- [31] M. Abed, M. A. Imteaz, and A. N. Ahmed, "Utilising Machine Learning for Pan Evaporation Prediction - A Case Study in Western Australia," *Lect. Notes Eng. Comput. Sci.*, vol. 2245, pp. 14–18, 2023.

Suryasatriya Trihandaru holds a Doctor of Mathematics degree from ITB,2005. He received his B.Sc. in Physics from Gadjah Mada University in Indonesia and M.Sc. (Industrial Mathematics) from Kaiserslautern University, in 1992 and 1998, respectively. In his master program he was a DAAD scholar, and sandwich program supported by DAAD, ICTP, and the Indonesian government scholar for his doctoral program. He is currently an associate professor in the Master of Data Science Department at Satva Wacana Christian University in Indonesia. He is one of the founders of Master program in Data Science in this university since 2020 and has been developing the application of artificial intelligence for mining and the internet of things for several purposes in some surrounding companies as a collaboration between the university and the industries. His research includes machine learning, artificial intelligence, internet of things, and medical physics. He has published over 10 papers in international journals and conferences in the last 5 years. He can be contacted at email: suryasatriya@uksw.edu.

Hanna Arini Parhusip is professor of applied mathematics in Master of Data Science, she holds a Doctor of Mathematics degree from ITB, 2005. She received her B.Sc. of Mathematics from Gadjah Mada University in Indonesia and her M.Sc. (Industrial Mathematics) from Kaiserslautern University, Germany in 1992 and 1997, respectively. In her master program, she was DAAD scholar, and the sandwich program, was supported by DAAD, ICTP, and the Indonesian government scholar for her doctor program. She has been one of the founders in the Master program in Data Science at this university since 2020 and has involved in several projects in applied mathematics with some surrounding companies as a collaboration between the university and the industries. She has published over 10 papers in international journals and conferences in the last 5 years. She has been the head of the Master program in Data Science. She can be contacted at email: hanna.parhusip@uksw.edu.

Devina Intan Sari holds a Bachelor of Science degree in Chemistry, graduating with cum laude honors in 2021 from Satya Wacana Christian University, Indonesia. She earned her Master's degree in Data Science from the same university in March 2025. She was one of the authors of a journal article on compound classification using Machine Learning and Neural Network. She can be contacted via email at devinais9906@gmail.com.